

In-plane chemical pressure essential for superconductivity in BiCh₂-based (Ch: S, Se) layered structure

Yoshikazu Mizuguchi^{1*}, Akira Miura², Joe Kajitani¹, Takafumi Hiroi¹, Osuke Miura¹, Kiyoharu Tadanaga², Nobuhiro Kumada³, Eisuke Magome⁴, Chikako Moriyoshi⁴, Yoshihiro Kuroiwa⁴

1. Department of Electrical and Electronic Engineering, Tokyo Metropolitan University, 1-1, Minami-osawa, Hachioji 192-0397, Japan.
2. Faculty of Engineering, Hokkaido University, Kita-13, Nishi-8, Kita-ku, Sapporo 060-8628 Japan.
3. Center for Crystal Science and Technology, University of Yamanashi, 7-32 Miyamae, Kofu 400-8511 Japan.
4. Department of Physical Science, Hiroshima University, 1-3-1 Kagamiyama, Higashihiroshima, Hiroshima 739-8526 Japan.

Abstract

BiCh₂-based superconductors (Ch: S, Se) are a new series of layered superconductor. However, mechanisms for the emergence of superconductivity in BiCh₂-based superconductors have not been clarified. In this study, we have investigated crystal structure of two series of optimally-doped BiCh₂-based superconductors, Ce_{1-x}Nd_xO_{0.5}F_{0.5}BiS₂ and LaO_{0.5}F_{0.5}Bi(S_{1-y}Se_y)₂, using powder synchrotron x-ray diffraction in order to reveal the relationship between crystal structure and superconducting properties of the BiCh₂-based family. We have found that an enhancement of in-plane chemical pressure would commonly induce bulk superconductivity in both systems. Furthermore, we have revealed that superconducting transition temperature for REO_{0.5}F_{0.5}BiCh₂ superconductors could universally be determined by degree of in-plane chemical pressure.

Most of superconductors with a high transition temperature (T_c) possess a layered crystal structure. Typical examples of layered high- T_c superconductor are Cu-oxide [1] and Fe-based superconductors [2]. They have a crystal structure composed of an alternate stacking of superconducting layers (CuO₂ or FeAs layers) and spacer layers. The spacer layers are electrically insulating and essential for the emergence of low-dimensional electronic states within the superconducting layers, which is sometimes responsible for the emergence of unconventional pairing mechanisms. One of the attractive features of those layered superconductors is a wide variation of crystal structure. Various kinds of new superconductors can be designed by stacking common superconducting layers and various types of spacer layers, and their superconducting properties depend on types of the spacer layers. In fact, many Fe-based superconductors with various types of spacer layer have been discovered, and high T_c was achieved in several Fe-based superconductors [2-8].

With a wide variation of related layered superconductors with various structures and properties, one can extract a crystal structure parameter essential for the emergence of superconductivity in the layered family. In the Fe-based family, it was found that T_c can be estimated by a crystal structure parameter such as an As-Fe-As bond angle [9] or an anion height from Fe square lattice (anion = As, P, Se, and Te) [10]. Changes in those parameters strongly affect configurations of Fermi surfaces and pairing symmetry, and superconducting properties of Fe-based superconductors [11]. In fact, clarification of a crystal structure correlating with superconducting properties is one of the most important challenges for understanding the mechanisms of superconductivity in a new series of layered superconductor. In addition, it gives a direct strategy for designing new layered superconductors with a higher T_c .

In 2012, we reported the discovery of novel layered superconductors with a crystal structure composed of an alternate stacking of common BiS₂ superconducting layers and various spacer layers [12,13]. Band calculations suggested that the parent phase of BiS₂-based superconductors is an insulator with Bi³⁺. Superconductivity is induced when electron carriers are doped into the BiS₂ layers (within Bi-6p orbitals) by element substitution at the spacer layers [12,14]. For example, a parent compound REOBiS₂ becomes a superconductor by a partial substitution of O at the spacer layers by F (namely, REO_{1-x}F_xBiS₂) [13]. So far, 12 kinds of parent compounds of BiS₂-based superconductor have been discovered: REOBiS₂ (RE = La [13], Ce [15], Pr [16], Nd [17], Sm [18], Yb [19], and Bi [20,21]), AFBiS₂ (A = Sr [22], Eu [23]), Bi₆O₈S₅ [12], Bi₃O₂S₃ [24], and Eu₃F₄Bi₂S₄ [25]. In addition, superconductivity was observed in a BiSe₂-based compound LaO_{0.5}F_{0.5}BiSe₂ as well [26]. Therefore, exploration for new BiCh₂-based (Ch:

S, Se) layered superconductors and studies with an aim to elucidate the mechanisms of superconductivity in the BiCh₂ layered compounds have attracted researchers in the field of condensed matter physics.

As mentioned above, electron-carrier doping is needed for the emergence of superconductivity in the BiCh₂ family. On the other front, some reports have suggested that optimization of crystal structure is also important for the emergence of superconductivity in the BiCh₂ family. One of those is a high pressure (HP) effect on T_c . For example, LaO_{0.5}F_{0.5}BiS₂ shows dramatic changes in superconductivity under HP. LaO_{0.5}F_{0.5}BiS₂ does not show bulk superconductivity while it shows a filamentary (weak) superconductivity signal with a T_c of 2.5 K [13]. With applying HP, LaO_{0.5}F_{0.5}BiS₂ becomes a bulk superconductor and T_c largely increases from 2.5 K to over 10 K [13,27-31]. In addition, an enhancement of T_c under HP was observed in other REO_{0.5}F_{0.5}BiS₂ superconductors as well [31]. These facts strongly suggest that superconducting properties of BiCh₂-based superconductors are correlated with changes in crystal structure as revealed in the Fe-based family [9,10].

Furthermore, our recent studies on isovalent-substitution effects to superconductivity have suggested that optimization of crystal structure is important for the emergence of bulk superconductivity and a higher T_c in optimally-doped REO_{0.5}F_{0.5}BiCh₂. One of the examples is Ce_{1-x}Nd_xO_{0.5}F_{0.5}BiS₂ [32]. Since valence of Ce and Nd are basically 3+ in this crystal structure, electron carriers in these compounds are essentially the same: a formal valence of Bi is 2.5+. However, bulk superconductivity is induced by a systematic substitution of Ce by Nd, and T_c increased with increasing Nd concentration (x) as shown in Fig. 1a. The emergence of superconductivity was explained by uniaxial lattice shrinkage along the a -axis and optimization of a lattice shrinkage ratio c / a [32]. The other example of the isovalent-substitution systems is LaO_{0.5}F_{0.5}Bi(S_{1-y}Se_y)₂ [33]. In LaO_{0.5}F_{0.5}Bi(S_{1-y}Se_y)₂, the S²⁻ site within the superconducting layers is systematically substituted by Se²⁻. Therefore, the formal valence of Bi^{2.5+} should not be changed by Se substitution. Bulk superconductivity is induced by Se substitution, and T_c increases with increasing Se concentration (y) as shown in Fig. 1b. In this system, Se substitution enhances metallic conductivity, and bulk superconductivity is induced by an expansion of lattice volume by Se substitution [33].

On the basis of these experimental facts in HP studies on REO_{0.5}F_{0.5}BiS₂ [13,27-31] and isovalent-substitution studies on Ce_{1-x}Nd_xO_{0.5}F_{0.5}BiS₂ and LaO_{0.5}F_{0.5}Bi(S_{1-y}Se_y)₂ [32,33], there is no doubt that superconducting properties of the BiCh₂ family correlate with not only electron carrier concentration but also their crystal

structure. However, universal relationship between crystal structure and the emergence of superconductivity (and their T_c) in the BiCh₂ family has not been clarified yet. In this study, we aim to clarify a crystal structure which directly correlates with the emergence of superconductivity and T_c of the BiCh₂ family. Fortunately, we have two isovalent-substitution systems of Ce_{1-x}Nd_xO_{0.5}F_{0.5}BiS₂ and LaO_{0.5}F_{0.5}Bi(S_{1-y}Se_y)₂, which exhibit a similar superconductivity phase diagram to each other as shown in Fig. 1. In order to discuss the changes in crystal structure parameters and their relationship to superconductivity, we have performed powder synchrotron x-ray diffraction (XRD) and Rietveld refinement for Ce_{1-x}Nd_xO_{0.5}F_{0.5}BiS₂ and LaO_{0.5}F_{0.5}Bi(S_{1-y}Se_y)₂.

Here, we show that an enhancement of in-plane chemical pressure within the superconducting Bi-Ch plane would be a crystal structure parameter, which commonly explain the emergence of superconductivity in REO_{0.5}F_{0.5}BiCh₂ compounds. Furthermore, we show that T_c for REO_{0.5}F_{0.5}BiCh₂ superconductors could universally be determined by degree of in-plane chemical pressure.

Results

Evolution of crystal structure parameters.

We have performed powder synchrotron XRD for Ce_{1-x}Nd_xO_{0.5}F_{0.5}BiS₂ and LaO_{0.5}F_{0.5}Bi(S_{1-y}Se_y)₂ and performed Rietveld refinement. Typical Rietveld refinement profiles for $x = 0.6$ and $y = 0.5$ are displayed in supplementary information (Figure S1). Although tiny impurity phases of RE fluorides were detected, all the XRD peaks of the main phase were refined using a tetragonal $P4/nmm$ space group. Obtained crystal structure parameters are plotted as a function of x (or y) in Fig. 2: the crystal structure data are listed in supplementary information (Table S2). In Fig. 2, the data points for the samples showing bulk superconductivity (Bulk SC) are highlighted with orange-filled circles. If a crystal structure parameter for Ce_{1-x}Nd_xO_{0.5}F_{0.5}BiS₂ and LaO_{0.5}F_{0.5}Bi(S_{1-y}Se_y)₂ changed similarly to each other, the crystal structure parameter should be essential for the emergence of superconductivity in these series because these two series exhibit a similar superconductivity phase diagram as a function of x or y as introduced in Fig. 1.

Figure 2a and 2b show the x (or y) dependences of lattice constants of a and c for Ce_{1-x}Nd_xO_{0.5}F_{0.5}BiS₂ and LaO_{0.5}F_{0.5}Bi(S_{1-y}Se_y)₂, respectively. In Ce_{1-x}Nd_xO_{0.5}F_{0.5}BiS₂, both lattice constants decrease with increasing x due to an increase in concentration of Nd³⁺ (112 pm, assuming coordination number of 8), which is smaller than Ce³⁺ (114 pm). In contrast, both lattice constants increase with increasing y in LaO_{0.5}F_{0.5}Bi(S_{1-y}Se_y)₂

due to an increase in concentration of Se^{2-} (198 pm, assuming coordination number of 6), which is larger than S^{2-} (184 pm). These contrasting changes in lattice constants suggest that the evolution of superconductivity in these two series cannot be explained by a simple lattice contraction or expansion.

Figure 2c shows the x (or y) dependences of Ch1-Bi-Ch1 angle for $\text{Ce}_{1-x}\text{Nd}_x\text{O}_{0.5}\text{F}_{0.5}\text{BiS}_2$ and $\text{LaO}_{0.5}\text{F}_{0.5}\text{Bi}(\text{S}_{1-y}\text{Se}_y)_2$. The Ch1-Bi-Ch1 angle is an indicator of flatness of Bi-Ch1 plane. Since electrons within the Bi-6p orbitals hybridized with the Ch-p orbitals (S-3p or Se-4p) are essential for the emergence of superconductivity in BiCh₂-based superconductors, a flatter Bi-Ch1 plane simply seems to be better for the emergence of bulk superconductivity with a higher T_c . In fact, a previous study on crystal structure of $\text{CeO}_{1-x}\text{F}_x\text{BiS}_2$ single crystals with different F concentrations indicated that a flatter Bi-S1 plane resulted in higher superconducting properties [34]. In $\text{Ce}_{1-x}\text{Nd}_x\text{O}_{0.5}\text{F}_{0.5}\text{BiS}_2$, the Ch1-Bi-Ch1 angle approaches 180 degree with increasing x , indicating that the Bi-S1 plane becomes flatter, and superconductivity is induced with Nd substitution. However, the Se concentration dependence of Ch1-Bi-Ch1 angle for $\text{LaO}_{0.5}\text{F}_{0.5}\text{Bi}(\text{S}_{1-y}\text{Se}_y)_2$ exhibits a contrasting behavior to that observed with Nd substitution effect in $\text{Ce}_{1-x}\text{Nd}_x\text{O}_{0.5}\text{F}_{0.5}\text{BiS}_2$. With increasing y , the Ch1-Bi-Ch1 angle decreases: the Bi-Ch1 plane becomes distorted. Therefore, the Ch1-Bi-Ch1 angle (flatness of the Bi-Ch1 plane) cannot commonly explain the evolution of superconductivity in BiCh₂-based superconductors. The contrasting changes in the in-plane structure (flatness) may be due to the difference in Ch²⁻ ions at the Ch1 site. Figure 2d shows the y dependence of occupancy of Se at the Ch1 site. As it is clear in Fig. 2d, Se ions selectively occupy the in-plane Ch1 site. At $x = 0.5$, approximately 90% of Ch1 site is occupied with Se. Recently, similar site selectivity of Se in $\text{LaO}_{1-x}\text{F}_x\text{BiSSe}$ single crystals were reported [35]. The preferential occupation of Se^{2-} with a larger ionic radius within the two-dimensional Bi-Ch1 plane may cause distortion.

Figure 2e shows the x (or y) dependences of three kinds of Bi-Ch distance. As depicted in a right-side image of the BiCh₂ layer, a Bi ion is coordinated by six Ch ions. The shortest Bi-Ch distance is the Bi-Ch2 distance toward a c -axis direction. The Bi-Ch2 distance for $\text{Ce}_{1-x}\text{Nd}_x\text{O}_{0.5}\text{F}_{0.5}\text{BiS}_2$ slightly decreases with increasing x . In contrast, the Bi-Ch2 distance for $\text{LaO}_{0.5}\text{F}_{0.5}\text{Bi}(\text{S}_{1-y}\text{Se}_y)_2$ increases with increasing y . Therefore, the Bi-Ch2 distance should not be essential for the evolution of superconductivity within these two series. Next, we discuss the in-plane Bi-Ch1 distance. The Bi-Ch1 (in-plane) distance for $\text{Ce}_{1-x}\text{Nd}_x\text{O}_{0.5}\text{F}_{0.5}\text{BiS}_2$ exhibits a decrease with increasing x . In contrast, the Bi-Ch1 (in-plane) distance for $\text{LaO}_{0.5}\text{F}_{0.5}\text{Bi}(\text{S}_{1-y}\text{Se}_y)_2$ increases with increasing y . These facts suggest that the in-plane Bi-Ch1 distance itself cannot explain the evolution of

superconductivity. The longest Bi-Ch distance is Bi-Ch1 (inter-plane), which is roughly corresponding to the inter-layer distance of two BiCh₂ layers. The Bi-Ch1 (inter-plane) distance for Ce_{1-x}Nd_xO_{0.5}F_{0.5}BiS₂ does not exhibit a remarkable change upon Nd substitution while that for LaO_{0.5}F_{0.5}Bi(S_{1-y}Se_y)₂ clearly increases with increasing *y*. Therefore, the Bi-Ch1 (inter-plane) distance cannot commonly explain the evolution of superconductivity.

Although we expected that a Ch1-Bi-C1 angle or some Bi-Ch distance exhibit a common behavior in Ce_{1-x}Nd_xO_{0.5}F_{0.5}BiS₂ and LaO_{0.5}F_{0.5}Bi(S_{1-y}Se_y)₂, we could not extract any clear correlation between them. However, we assumed that the in-plane Bi-Ch1 distance should correlate with the evolution of superconductivity to a certain extent because the superconductivity is induced within the Bi-Ch1 plane, and their superconducting properties dramatically change by changing the crystal structure without changes in electron carrier concentration (F concentration). Therefore, we introduce a concept of *in-plane chemical pressure* to discuss the relationship between in-plane structure and evolution of superconductivity in Ce_{1-x}Nd_xO_{0.5}F_{0.5}BiS₂, LaO_{0.5}F_{0.5}Bi(S_{1-y}Se_y)₂, and other REO_{0.5}F_{0.5}BiCh₂ superconductors.

Emergence of superconductivity by in-plane chemical pressure.

Figure 3a shows schematic images of compression or expansion of Bi-Ch plane by Nd or Se substitution. In the case of Ce_{1-x}Nd_xO_{0.5}F_{0.5}BiS₂, Bi-Ch1 planes are compressed according to a decrease in volume of spacer layers with increasing Nd concentration (*x*). The compression of Bi-Ch1 plane results in an enhancement of packing density of Bi^{2.5+} and S²⁻ ions within the superconducting plane: this is so-called *in-plane chemical pressure*. In the case of LaO_{0.5}F_{0.5}Bi(S_{1-y}Se_y)₂, the in-plane Bi-Ch1 distance increases with increasing occupancy of Se at the Ch1 site. However, the expansion of the in-plane Bi-Ch1 distance is smaller than that simply expected from the difference in ionic radius of S²⁻ and Se²⁻ because the component of the spacer layer (LaO) never changes in LaO_{0.5}F_{0.5}Bi(S_{1-y}Se_y)₂. Therefore, the packing density of Bi^{2.5+} and Ch²⁻ ions within the superconducting plane is enhanced. This situation is actually similar to the enhancement of in-plane chemical pressure in Ce_{1-x}Nd_xO_{0.5}F_{0.5}BiS₂. In order to compare degree of in-plane chemical pressure of two series, we define a value of in-plane chemical pressure using equation (1).

$$\text{In-plane chemical pressure} = (R_{\text{Bi}} + R_{\text{Ch1}}) / \text{Bi-Ch1(in-plane)} \quad (1)$$

R_{Bi} is an ionic radius of Bi^{2.5+}. Here, we assumed that the ionic radius of Bi^{2.5+} is 104.19

pm, which is obtained from the average of the six Bi-S bonds (four in-plane Bi-S1 bonds, one inter-plane Bi-S1 bond, and one Bi-S2 bond) determined from a crystal structure analysis with a single crystal of $\text{LaO}_{0.54}\text{F}_{0.46}\text{BiS}_2$ [36]. R_{Ch1} is an ionic radius of chalcogen at the Ch1 site: 184 and 198 pm for S^{2-} and Se^{2-} , respectively. In the case of $\text{LaO}_{0.5}\text{F}_{0.5}\text{Bi}(\text{S}_{1-y}\text{Se}_y)_2$, we calculated an average value for R_{Ch1} using occupancy of Se at the Ch1 site. The Bi-Ch1 (in-plane) is the data obtained from Rietveld refinement (Fig. 2e). We note that chemical pressure derived from ionic radii is a simple estimation, and it cannot describe exact orbital overlap between Bi and Ch. However, the assumption looks very useful to discuss the relationship between crystal structure and superconductive properties of these systems.

The calculated in-plane chemical pressure is plotted as a function of x (or y) in Fig. 3b. For both systems, in-plane chemical pressure increases with increasing x (or y). Surprisingly, the chemical pressure, at which bulk superconductivity is induced, is almost the same (above ~ 1.011) in between $\text{Ce}_{1-x}\text{Nd}_x\text{O}_{0.5}\text{F}_{0.5}\text{BiS}_2$ and $\text{LaO}_{0.5}\text{F}_{0.5}\text{Bi}(\text{S}_{1-y}\text{Se}_y)_2$. On the basis of these experimental facts, we suggest that the emergence of bulk superconductivity in both $\text{Ce}_{1-x}\text{Nd}_x\text{O}_{0.5}\text{F}_{0.5}\text{BiS}_2$ and $\text{LaO}_{0.5}\text{F}_{0.5}\text{Bi}(\text{S}_{1-y}\text{Se}_y)_2$ systems can commonly be explained by the increase of in-plane chemical pressure. The enhancement of in-plane chemical pressure should enhance the overlaps of Bi-6p and Ch-p orbitals. The enhancement of orbital overlaps would result in an enhancement of metallic conductivity and an inducement of bulk superconductivity in $\text{REO}_{0.5}\text{F}_{0.5}\text{BiCh}_2$ family. In the discussion part, we discuss the relationship between T_c and in-plane chemical pressure within the Bi-Ch1 plane.

Discussion

To discuss the relationship between T_c and in-plane chemical pressure, we plotted T_c for $\text{Ce}_{1-x}\text{Nd}_x\text{O}_{0.5}\text{F}_{0.5}\text{BiS}_2$ and $\text{LaO}_{0.5}\text{F}_{0.5}\text{Bi}(\text{S}_{1-y}\text{Se}_y)_2$ as a function of in-plane chemical pressure in Fig. 4. To obtain a general tendency in $\text{REO}_{0.5}\text{F}_{0.5}\text{BiCh}_2$ superconductors, we added data points for $\text{Nd}_{0.8}\text{Sm}_{0.2}\text{O}_{0.5}\text{F}_{0.5}\text{BiS}_2$ and $\text{Nd}_{0.6}\text{Sm}_{0.4}\text{O}_{0.5}\text{F}_{0.5}\text{BiS}_2$ [analyzed in this study], $\text{NdO}_{0.5}\text{F}_{0.5}\text{BiS}_2$ single crystal [37], $\text{PrO}_{0.5}\text{F}_{0.5}\text{BiS}_2$ [16], $\text{SmO}_{0.5}\text{F}_{0.5}\text{BiS}_2$ single crystal [18], and $\text{LaO}_{0.5}\text{F}_{0.5}\text{BiSe}_2$ ($y = 1$) single crystal [38]. Interestingly, data points for all the $\text{REO}_{0.5}\text{F}_{0.5}\text{BiS}_2$ -type are located on a single slope highlighted by a blue region. Notably, the data points for $\text{CeO}_{0.5}\text{F}_{0.5}\text{BiS}_2$ and $\text{SmO}_{0.5}\text{F}_{0.5}\text{BiS}_2$, which do not exhibit superconductivity, locate on the left region of the boundary suggested in Fig. 4 (in-plane chemical pressure < 1.011). These facts suggest that the emergence of superconductivity and T_c of $\text{REO}_{0.5}\text{F}_{0.5}\text{BiS}_2$ -type simply depend on

degree of in-plane chemical pressure. The enhancement of overlap between Bi-6p and Ch-p orbitals should enhance density of state near the Fermi level. If we assume the BCS theory [39], the enhancement of T_c with increasing in-plane chemical pressure can be understood by the enhancement of density of state at the Fermi level. On the other hand, T_c for $\text{LaO}_{0.5}\text{F}_{0.5}\text{Bi}(\text{S}_{1-y}\text{Se}_y)_2$ and LaOBiSe_2 , indicated with a red region, are clearly located on a lower side of that for the $\text{REO}_{0.5}\text{F}_{0.5}\text{BiS}_2$ -type series. As an important fact, evolutions of T_c in $\text{REO}_{0.5}\text{F}_{0.5}\text{BiS}_2$ and $\text{LaO}_{0.5}\text{F}_{0.5}\text{Bi}(\text{S}_{1-y}\text{Se}_y)_2$ do not correspond and exhibit different curves. For the $\text{LaO}_{0.5}\text{F}_{0.5}\text{Bi}(\text{S}_{1-y}\text{Se}_y)_2$ compounds, in-plane chemical pressure is relatively stronger than that in $\text{REO}_{0.5}\text{F}_{0.5}\text{BiS}_2$, but their T_c is clearly lower than those of $\text{REO}_{0.5}\text{F}_{0.5}\text{BiS}_2$. As described above, Se preferably occupies the in-plane Ch1 site. Therefore, it can be considered that superconductivity in $\text{LaO}_{0.5}\text{F}_{0.5}\text{Bi}(\text{S}_{1-y}\text{Se}_y)_2$ is induced in a Bi-(S,Se) or a Bi-Se plane. If we assume the BCS theory again, the lower T_c in Bi-Se plane can be explained by a lower phonon frequency in Bi-Se plane than that in Bi-S plane due to the larger atomic number of Se. If we could obtain other $\text{REO}_{0.5}\text{F}_{0.5}\text{BiSe}_2$ superconductors like $\text{CeO}_{0.5}\text{F}_{0.5}\text{BiSe}_2$ or $\text{NdO}_{0.5}\text{F}_{0.5}\text{BiSe}_2$ and add data points on an extension of the $\text{LaO}_{0.5}\text{F}_{0.5}\text{Bi}(\text{S}_{1-y}\text{Se}_y)_2$ series, we can confirm the assumption above. With Fig. 4, we expect that a higher T_c would be obtained with Bi-S plane with a higher in-plane chemical pressure in $\text{REO}_{0.5}\text{F}_{0.5}\text{BiCh}_2$ -type compounds.

At the end, we briefly discuss about the HP phase of $\text{LaO}_{0.5}\text{F}_{0.5}\text{BiS}_2$ which shows the highest T_c among BiCh₂-based superconductors [27-31]. T. Tomita *et al.* reported that the crystal structure of $\text{LaO}_{0.5}\text{F}_{0.5}\text{BiS}_2$ above 0.7 GPa was monoclinic [30]. In the monoclinic structure, the Bi-S1 plane is distorted into a zigzag chain with a shorter Bi-S1 distance of 2.72 Å; zigzag chains are connected with a longer Bi-S1 distance of 3.03 Å to each other. In fact, we reported in-plane anisotropy of upper critical field within the Bi-S1 plane in a HP phase of $\text{LaO}_{0.5}\text{F}_{0.5}\text{BiS}_2$, implying the emergence of quasi-one-dimensional superconducting states within the distorted Bi-S1 plane of a HP phase of $\text{LaO}_{0.5}\text{F}_{0.5}\text{BiS}_2$ [40]. If we simply calculate the value of chemical pressure using a Bi-S1 distance of 2.72 Å with the equation (1), we obtain chemical pressure of 1.06. (In this case, obtained chemical pressure is not in-plane chemical pressure but quasi-one-dimensional chemical pressure.) Chemical pressure of 1.06 and T_c of 10 K give a data point locating on a rough extension of the T_c -chemical pressure curve for the other $\text{REO}_{0.5}\text{F}_{0.5}\text{BiS}_2$ superconductors discussed in Fig. 4. This might indicate that the enhancement of quasi-one-dimensional chemical pressure, not in-plane chemical pressure, would be essential for the evolution of superconductivity in $\text{REO}_{0.5}\text{F}_{0.5}\text{BiCh}_2$ compounds. To further discuss and understand the relationship between chemical pressure and superconductivity in the BiCh₂ family, investigations of crystal structure

and superconducting properties for new BiS₂-, BiSe₂-based and/or BiTe₂-based compounds with various spacer layers are needed.

In summary, we have analyzed crystal structure of optimally-doped BiCh₂-based superconductors Ce_{1-x}Nd_xO_{0.5}F_{0.5}BiS₂ and LaO_{0.5}F_{0.5}Bi(S_{1-y}Se_y)₂ using powder synchrotron XRD to reveal relationship between crystal structure and superconducting properties in BiCh₂-based layered compounds. We have found that the enhancement of in-plane chemical pressure could commonly induce bulk superconductivity in both systems. Furthermore, we revealed that T_c for the REO_{0.5}F_{0.5}BiCh₂ superconductors could be determined by degree of in-plane chemical pressure and a kind of Ch element composing superconducting Bi-Ch planes. In addition, on the basis of discussion on the relationship between chemical pressure and superconductivity in REO_{0.5}F_{0.5}BiCh₂ compounds and a monoclinic phase (high pressure phase) of LaO_{0.5}F_{0.5}BiS₂, we suggest a possibility that the enhancement of quasi-one-dimensional chemical pressure within a Bi-Ch chain, not in-plane (two-dimensional) chemical pressure, would be essential for a higher T_c in BiCh₂-based superconductors.

Methods

Polycrystalline samples of Ce_{1-x}Nd_xO_{0.5}F_{0.5}BiS₂ and LaO_{0.5}F_{0.5}Bi(S_{1-y}Se_y)₂ used in this study were prepared using solid state reaction. The detailed synthesis procedures were described in previous reports [32,33]. Powder synchrotron X-ray powder diffraction measurements were performed at room temperature at the BL02B2 experimental station of SPring-8 (JASRI; Proposal No. 2014B1003 and 2014B1071). The wavelength of the radiation beam was 0.49542(4) Å. We have performed the Rietveld refinement (RIETAN-FP [41]) for Ce_{1-x}Nd_xO_{0.5}F_{0.5}BiS₂ and LaO_{0.5}F_{0.5}Bi(S_{1-y}Se_y)₂ using a typical structure model of REOBiCh₂-based superconductor with a tetragonal space group of *P4/nmm* [35,36]. Contributions from impurity phases of rare-earth fluorides (REF₃) and/or Bi₂S₃ are included in Rietveld refinement. In addition, we have analyzed a crystal structure for two related compounds of Nd_{0.8}Sm_{0.2}O_{0.5}F_{0.5}BiS₂ and Nd_{0.6}Sm_{0.4}O_{0.5}F_{0.5}BiS₂ to enrich the discussion part [32]. The obtained crystal structure parameters are summarized in Table S1. The schematic images of crystal structure were drawn using VESTA [42].

Acknowledgements

The authors would like to thank Dr. N. L. Saini of Sapienza University of Rome, Dr. K.

Kuroki of Osaka University and Dr. Y. Takano of National Institute for Materials Science for fruitful discussion. This work was partly supported by Grant-in-Aid for Young Scientist (A): 25707031 and Grant-in-Aid for challenging Exploratory Research: 26600077. The synchrotron x-ray diffraction were performed under proposals of JASRI; Proposal No. 2014B1003 and 2014B1071.

Author contributions

Y.M. and A.M. planned the research. Y.M., J.K., T.H and O.M. prepared polycrystalline samples and studied superconducting properties. Y.M., A.M., K.T., N.K., E.M., C.M. and Y.K. performed synchrotron XRD and crystal structure analysis. Y.M. wrote the manuscript.

References

- [1] Bednorz, J. G. & Müller, K. A. Possible high T_c superconductivity in the Ba-La-Cu-O system. *Z. Physik B Condensed Matter* **64**, 189-193 (1986).
- [2] Kamihara, Y. *et al.*, Iron-Based Layered Superconductor $\text{La}[\text{O}_{1-x}\text{F}_x]\text{FeAs}$ ($x=0.05-0.12$) with $T_c = 26$ K. *J. Am. Chem. Soc.* **130**, 3296–3297 (2008).
- [3] Chen, X. H. *et al.*, Superconductivity at 43 K in $\text{SmFeAsO}_{1-x}\text{F}_x$. *Nature* **453**, 761-762 (2008).
- [4] Ren, Z. A. *et al.*, Superconductivity at 55 K in Iron-Based F-Doped Layered Quaternary Compound $\text{Sm}[\text{O}_{1-x}\text{F}_x]\text{FeAs}$. *Chinese Phys. Lett.* **25**, 2215 (2008).
- [5] Rotter, M., Tegel, M. & Johrendt, D. Superconductivity at 38 K in the Iron Arsenide $(\text{Ba}_{1-x}\text{K}_x)\text{Fe}_2\text{As}_2$. *Phys. Rev. Lett.* **101**, 107006(1-4) (2008).
- [6] Wang, X.C. *et al.*, The superconductivity at 18 K in LiFeAs system. *Solid State Commun.* **148**, 538–540 (2008).
- [7] Ogino, H. *et al.*, Superconductivity at 17 K in $(\text{Fe}_2\text{P}_2)(\text{Sr}_4\text{Sc}_2\text{O}_6)$: a new superconducting layered pnictide oxide with a thick perovskite oxide layer. *Supercond. Sci. Technol.* **22**, 075008(1-4) (2009).
- [8] Zhu, X. *et al.*, Transition of stoichiometric $\text{Sr}_2\text{VO}_3\text{FeAs}$ to a superconducting state at 37.2 K. *Phys. Rev. B* **79**, 220512(1-4) (2009).
- [9] Lee, C. H. *et al.*, Effect of Structural Parameters on Superconductivity in Fluorine-Free LnFeAsO_{1-y} ($\text{Ln} = \text{La}, \text{Nd}$). *J. Phys. Soc. Jpn.* **77**, 083704(1-4) (2008).
- [10] Mizuguchi, Y. *et al.*, Anion height dependence of T_c for the Fe-based superconductor. *Supercond. Sci. Technol.* **23**, 054013(1-5) (2010).

- [11] Kuroki, K. *et al.*, Pnictogen height as a possible switch between high- T_c nodeless and low- T_c nodal pairings in the iron-based superconductors. *Phys. Rev. B* **79**, 224511(1-16) (2009).
- [12] Mizuguchi, Y. *et al.*, BiS₂-based layered superconductor Bi₄O₄S₃. *Phys. Rev. B* **86**, 220510(1-5) (2012).
- [13] Mizuguchi, Y. *et al.*, Superconductivity in Novel BiS₂-Based Layered Superconductor LaO_{1-x}F_xBiS₂. *J. Phys. Soc. Jpn.* **81**, 114725(1-5) (2012).
- [14] Usui, H., Suzuki, K. & Kuroki, K., Minimal electronic models for superconducting BiS₂ layers. *Phys. Rev. B* **86**, 220501(1-5) (2012).
- [15] Xing, J. *et al.*, Superconductivity Appears in the Vicinity of an Insulating-Like Behavior in CeO_{1-x}F_xBiS₂. *Phys. Rev. B* **86**, 214518(1-5) (2012).
- [16] Jha, R. *et al.*, Synthesis and superconductivity of new BiS₂ based superconductor PrO_{0.5}F_{0.5}BiS₂. *J. Supercond. Nov. Magn.* **26**, 499-502 (2013).
- [17] Demura, S. *et al.*, BiS₂-based superconductivity in F-substituted NdOBiS₂. *J. Phys. Soc. Jpn.* **82**, 033708(1-3) (2013).
- [18] Thakur, G. S. *et al.*, Synthesis and properties of SmO_{0.5}F_{0.5}BiS₂ and enhancement in T_c in La_{1-y}Sm_yO_{0.5}F_{0.5}BiS₂. *Inorg. Chem.* **54**, 1076-1081 (2015).
- [19] Yazici, D. *et al.*, Superconductivity of F-substituted LnOBiS₂ (Ln=La, Ce, Pr, Nd, Yb) compounds. *Philos. Mag.* **93**, 673(1-8) (2012).
- [20] Okada, T. *et al.*, Topotactic Synthesis of a new BiS₂-based superconductor Bi₂(O,F)S₂. *Appl. Phys. Express* **8**, 023102(1-4) (2015).
- [21] Shao, J. *et al.*, Superconductivity in BiO_{1-x}F_xBiS₂ and possible parent phase of Bi₄O₄S₃ superconductor. *Supercond. Sci. Technol.* **28**, 015008(1-6) (2015).
- [22] Lin, X. *et al.*, Superconductivity induced by La doping in Sr_{1-x}La_xFBiS₂. *Phys. Rev. B* **87**, 020504(1-4) (2013).
- [23] Zhai, H. F. *et al.*, Possible Charge-density wave, superconductivity and f-electron valence instability in EuBiS₂F. *Phys. Rev. B* **90**, 064518(1-9) (2014).
- [24] Phelan, W. A. *et al.*, Stacking Variants and Superconductivity in the Bi-O-S System. *J. Am. Chem. Soc.* **135**, 5372-5374 (2013).
- [25] Zhai, H. F. *et al.*, Anomalous Eu Valence State and Superconductivity in Undoped Eu₃Bi₂S₄F₄. *J. Am. Chem. Soc.* **136**, 15386-15393 (2014).
- [26] Maziopa, A. K. *et al.*, Superconductivity in a new layered bismuth oxyselenide: LaO_{0.5}F_{0.5}BiSe₂. *J. Phys.: Condens. Matter* **26**, 215702(1-5) (2014).
- [27] Deguchi, K. *et al.*, Evolution of superconductivity in LaO_{1-x}F_xBiS₂ prepared by high pressure technique. *EPL* **101**, 17004(p1-p5) (2013).
- [28] Mizuguchi, Y. *et al.*, Stabilization of High- T_c Phase of BiS₂-Based Superconductor

- LaO_{0.5}F_{0.5}BiS₂ Using High-Pressure Synthesis. *J. Phys. Soc. Jpn.* **83**, 053704(1-4) (2014).
- [29] Kotegawa, H. *et al.*, Pressure Study of BiS₂-Based Superconductors Bi₄O₄S₃ and La(O,F)BiS₂. *J. Phys. Soc. Jpn.* **81**, 103702(1-4) (2012).
- [30] Tomita, T. *et al.*, Pressure-Induced Enhancement of Superconductivity and Structural Transition in BiS₂-Layered LaO_{1-x}F_xBiS₂. *J. Phys. Soc. Jpn.* **83**, 063704(1-4) (2014).
- [31] Wolowiec, C. T. *et al.*, Enhancement of superconductivity near the pressure-induced semiconductor–metal transition in the BiS₂-based superconductors LnO_{0.5}F_{0.5}BiS₂ (Ln = La, Ce, Pr, Nd). *J. Phys.: Condens. Matter* **25**, 42220(1-6) (2013).
- [32] Kajitani, J. *et al.*, Chemical pressure effect on superconductivity of BiS₂-based Ce_{1-x}Nd_xO_{1-y}F_yBiS₂ and Nd_{1-z}Sm_zO_{1-y}F_yBiS₂. *J. Phys. Soc. Jpn.* **84**, 044712(1-6) (2015).
- [33] Hiroi, T. *et al.*, Evolution of superconductivity in BiS₂-based superconductor LaO_{0.5}F_{0.5}Bi(S_{1-x}Se_x)₂. *J. Phys. Soc. Jpn.* **84**, 024723(1-4) (2015).
- [34] Miura, A. *et al.*, Structure, Superconductivity, and Magnetism of Ce(O,F)BiS₂ Single Crystals. *Cryst. Growth Des.* **15**, 39–44 (2015).
- [35] Tanaka, M. *et al.*, Site Selectivity on Chalcogen Atoms in Superconducting La(O,F)BiSSe. *Appl. Phys. Lett.* **106**, 112601(1-5) (2015).
- [36] Miura, A. *et al.*, Crystal structures of LaO_{1-x}F_xBiS₂ (x ~ 0.23, 0.46): effect of F doping on distortion of Bi-S plane. *J. Solid State Chem.* **212**, 213-217 (2014).
- [37] Nagao, M. *et al.*, Structural Analysis and Superconducting Properties of F-Substituted NdOBiS₂ Single Crystals. *J. Phys. Soc. Jpn.* **82**, 113701(1-4) (2013).
- [38] Tanaka, M. *et al.*, First single crystal growth and structural analysis of superconducting layered bismuth oxyselenide; La(O,F)BiSe₂. *J. Solid State Chem.* **219**, 168-172 (2014).
- [39] Bardeen, J., Cooper, L. N. & Schrieffer, J. R., Theory of Superconductivity. *Phys. Rev.* **108**, 1175-1204 (1957).
- [40] Mizuguchi, Y. *et al.*, Anisotropic upper critical field of BiS₂-based superconductor LaO_{0.5}F_{0.5}BiS₂. *Phys. Rev. B* **89**, 174515(1-7) (2014).
- [41] Izumi, F. & Momma, Three-Dimensional Visualization in Powder Diffraction. *Solid State Phenom.* **130**, 15-20 (2007).
- [42] Momma, K. & Izumi, F., VESTA: a three-dimensional visualization system for electronic and structural analysis. *J. Appl. Crystallogr.* **41**, 653-658 (2008).

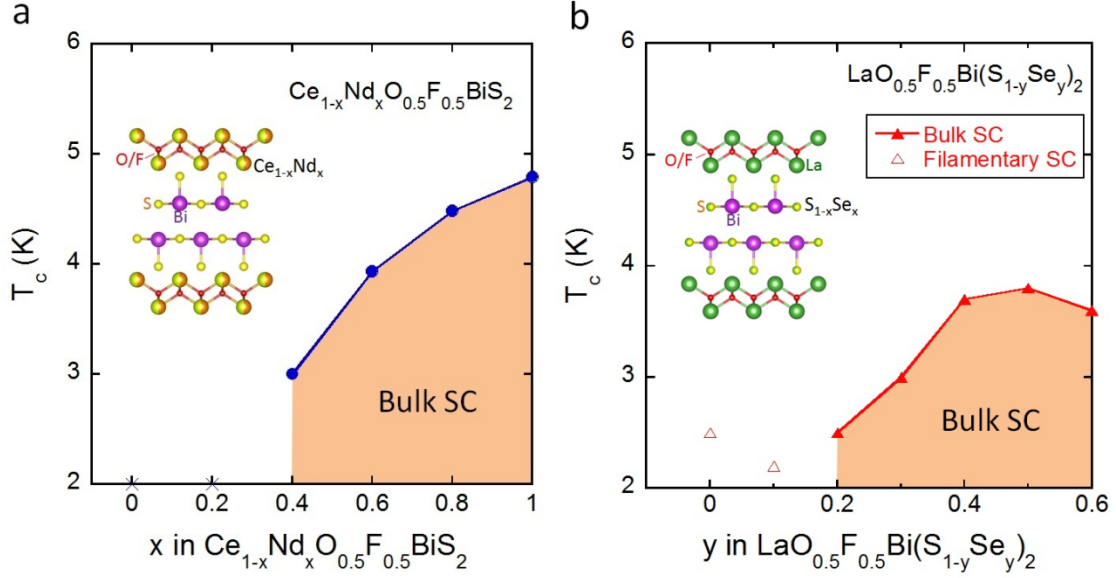


Fig. 1. Superconductivity phase diagrams of $\text{Ce}_{1-x}\text{Nd}_x\text{O}_{0.5}\text{F}_{0.5}\text{BiS}_2$ and $\text{LaO}_{0.5}\text{F}_{0.5}\text{Bi}(\text{S}_{1-y}\text{Se}_y)_2$.

a. Superconductivity phase diagrams of $\text{Ce}_{1-x}\text{Nd}_x\text{O}_{0.5}\text{F}_{0.5}\text{BiS}_2$. For $x = 0$ and 0.2 , superconducting transition is not observed at $T > 2$ K. For $0.4 \leq x \leq 1$, superconducting transition with a large shielding signal, with which we could regard the samples as a bulk superconductor (Bulk SC), is observed. T_c increases with increasing x . An inset figure shows a schematic image of crystal structure of $\text{Ce}_{1-x}\text{Nd}_x\text{O}_{0.5}\text{F}_{0.5}\text{BiS}_2$.

b. Superconductivity phase diagrams of $\text{LaO}_{0.5}\text{F}_{0.5}\text{Bi}(\text{S}_{1-y}\text{Se}_y)_2$. For $y = 0$ and 0.1 , superconducting transition is observed but their shielding signals are very small as a bulk superconductor (Filamentary SC). For $y \geq 0.2$, superconducting transition with a large shielding signal is observed (Bulk SC). T_c increases with increasing y up to $y = 0.5$. An inset figure shows a schematic image of crystal structure of $\text{LaO}_{0.5}\text{F}_{0.5}\text{Bi}(\text{S}_{1-y}\text{Se}_y)_2$.

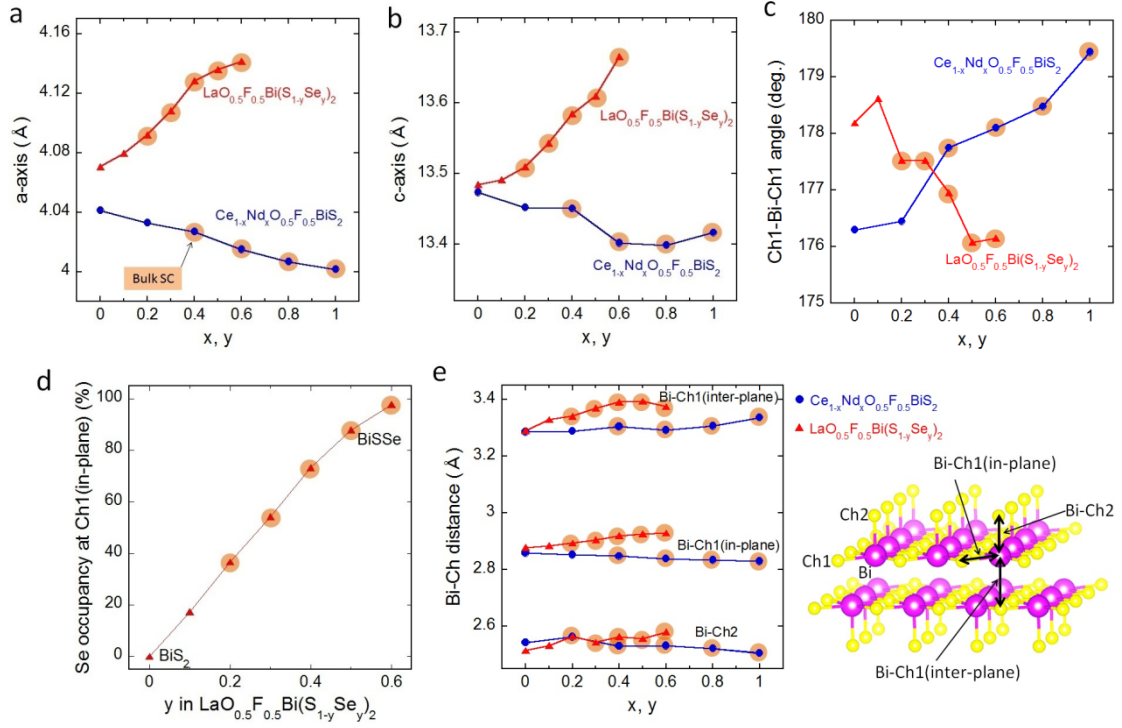


Fig. 2. Crystal structure parameters for $\text{Ce}_{1-x}\text{Nd}_x\text{O}_{0.5}\text{F}_{0.5}\text{BiS}_2$ and $\text{LaO}_{0.5}\text{F}_{0.5}\text{Bi}(\text{S}_{1-y}\text{Se}_y)_2$.

a. Lattice constant of a for $\text{Ce}_{1-x}\text{Nd}_x\text{O}_{0.5}\text{F}_{0.5}\text{BiS}_2$ and $\text{LaO}_{0.5}\text{F}_{0.5}\text{Bi}(\text{S}_{1-y}\text{Se}_y)_2$ is plotted as a function of x (or y). Data points for the samples showing bulk superconductivity (Bulk SC in Fig. 1) are highlighted with orange-filled circles in Figs. 2a-2e.

b. Lattice constant of c for $\text{Ce}_{1-x}\text{Nd}_x\text{O}_{0.5}\text{F}_{0.5}\text{BiS}_2$ and $\text{LaO}_{0.5}\text{F}_{0.5}\text{Bi}(\text{S}_{1-y}\text{Se}_y)_2$ is plotted as a function of x (or y).

c. Evolution of Ch1-Bi-Ch1 angle for $\text{Ce}_{1-x}\text{Nd}_x\text{O}_{0.5}\text{F}_{0.5}\text{BiS}_2$ and $\text{LaO}_{0.5}\text{F}_{0.5}\text{Bi}(\text{S}_{1-y}\text{Se}_y)_2$ as a function of x (or y).

d. Se concentration (y) dependence of occupancy of Se at the Ch1 site in the Bi-Ch1 plane for $\text{LaO}_{0.5}\text{F}_{0.5}\text{Bi}(\text{S}_{1-y}\text{Se}_y)_2$.

e. Evolution of three kinds of Bi-Ch distance for $\text{Ce}_{1-x}\text{Nd}_x\text{O}_{0.5}\text{F}_{0.5}\text{BiS}_2$ and $\text{LaO}_{0.5}\text{F}_{0.5}\text{Bi}(\text{S}_{1-y}\text{Se}_y)_2$ as a function of x (or y). The right crystal structure image describes the Bi, Ch1 and Ch2 sites, and three Bi-Ch distances: Bi-Ch1 (in-plane), Bi-Ch1 (inter-plane), and Bi-Ch2.

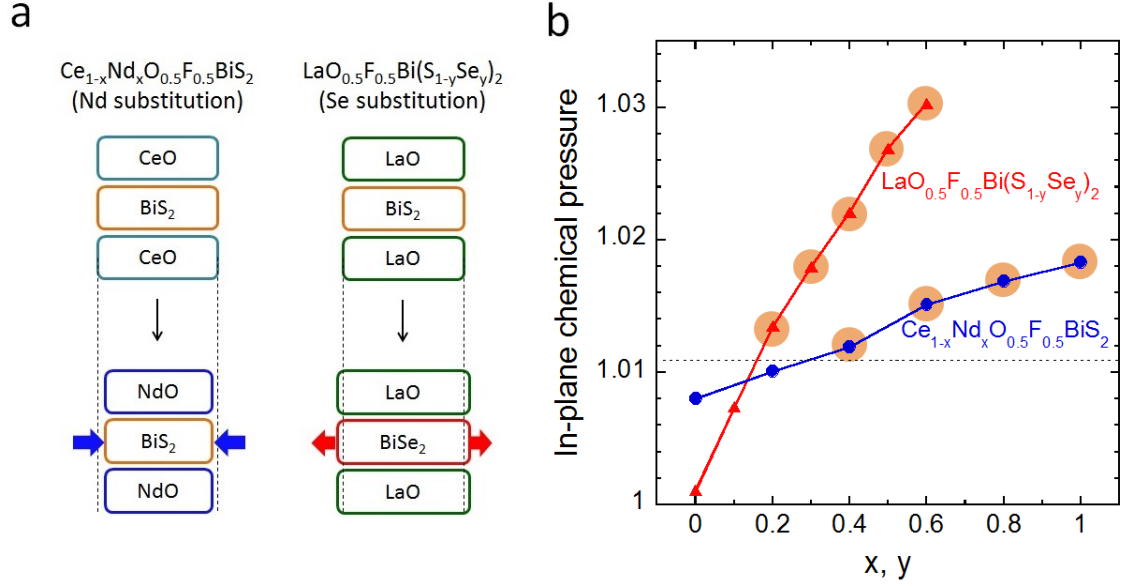


Fig. 3. Effect of in-plane chemical pressure to superconductivity in $\text{Ce}_{1-x}\text{Nd}_x\text{O}_{0.5}\text{F}_{0.5}\text{BiS}_2$ and $\text{LaO}_{0.5}\text{F}_{0.5}\text{Bi}(\text{S}_{1-y}\text{Se}_y)_2$.

a. Schematic image of changes in crystal structure with increasing in-plane chemical pressure in $\text{Ce}_{1-x}\text{Nd}_x\text{O}_{0.5}\text{F}_{0.5}\text{BiS}_2$ and $\text{LaO}_{0.5}\text{F}_{0.5}\text{Bi}(\text{S}_{1-y}\text{Se}_y)_2$. In $\text{Ce}_{1-x}\text{Nd}_x\text{O}_{0.5}\text{F}_{0.5}\text{BiS}_2$, a volume of spacer layer decreases with increasing Nd concentration (x), and Bi-S plane is compressed; hence, in-plane chemical pressure is enhanced. In $\text{LaO}_{0.5}\text{F}_{0.5}\text{Bi}(\text{S}_{1-y}\text{Se}_y)_2$, a volume of superconducting Bi-Ch1 layer increases with increasing Se concentration (y). However, the expansion of Bi-Ch1 plane is smaller than that expected from the ionic radius of S^{2-} and Se^{2-} because the component of the spacer layer (LaO layer) does not change; hence, in-plane chemical pressure is enhanced as well as in $\text{Ce}_{1-x}\text{Nd}_x\text{O}_{0.5}\text{F}_{0.5}\text{BiS}_2$.

b. In-plane chemical pressure for $\text{Ce}_{1-x}\text{Nd}_x\text{O}_{0.5}\text{F}_{0.5}\text{BiS}_2$ and $\text{LaO}_{0.5}\text{F}_{0.5}\text{Bi}(\text{S}_{1-y}\text{Se}_y)_2$, calculated using the equation (1), are plotted as a function of x (or y). In both systems, bulk superconductivity is induced with increasing chemical pressure. The dashed line at an in-plane chemical pressure of ~ 1.011 is an estimated boundary of bulk-SC and non-SC regions.

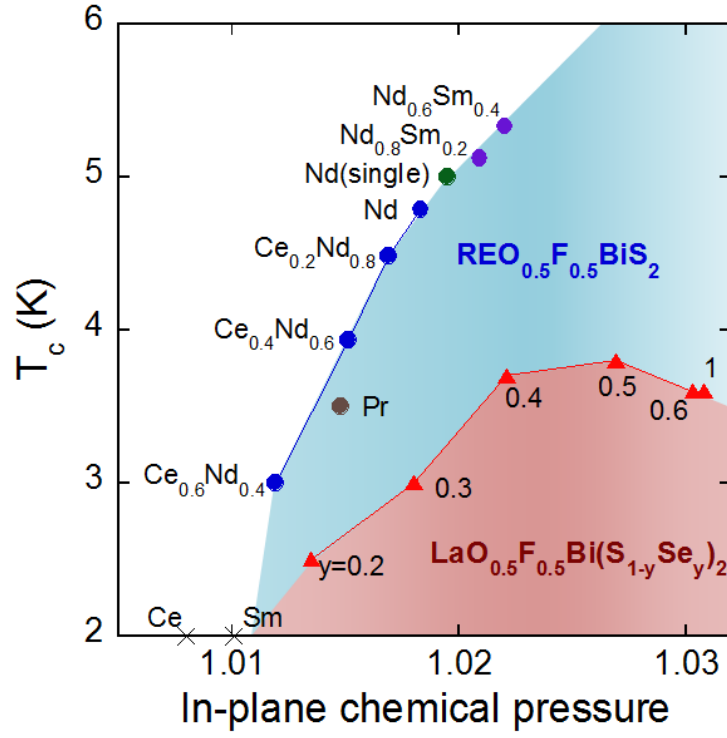


Fig. 4. Relationship between T_c and degree of in-plane chemical pressure in $\text{REO}_{0.5}\text{F}_{0.5}\text{BiS}_2$.

The data of T_c and in-plane chemical pressure for $\text{Ce}_{1-x}\text{Nd}_x\text{O}_{0.5}\text{F}_{0.5}\text{BiS}_2$ and $\text{LaO}_{0.5}\text{F}_{0.5}\text{Bi}(\text{S}_{1-y}\text{Se}_y)_2$ are plotted with those for $\text{Nd}_{0.8}\text{Sm}_{0.2}\text{O}_{0.5}\text{F}_{0.5}\text{BiS}_2$ and $\text{Nd}_{0.6}\text{Sm}_{0.4}\text{O}_{0.5}\text{F}_{0.5}\text{BiS}_2$ [analyzed in this work], $\text{NdO}_{0.5}\text{F}_{0.5}\text{BiS}_2$ single crystal [37], $\text{PrO}_{0.5}\text{F}_{0.5}\text{BiS}_2$ [16], $\text{SmO}_{0.5}\text{F}_{0.5}\text{BiS}_2$ single crystal [18], and $\text{LaO}_{0.5}\text{F}_{0.5}\text{BiSe}_2$ ($y = 1$) single crystal [38]. The data points of $\text{REO}_{0.5}\text{F}_{0.5}\text{BiS}_2$ and those of $\text{LaO}_{0.5}\text{F}_{0.5}\text{Bi}(\text{S}_{1-y}\text{Se}_y)_2$ exhibit different curves as separated by blue and red regions, respectively.

Supplementary information

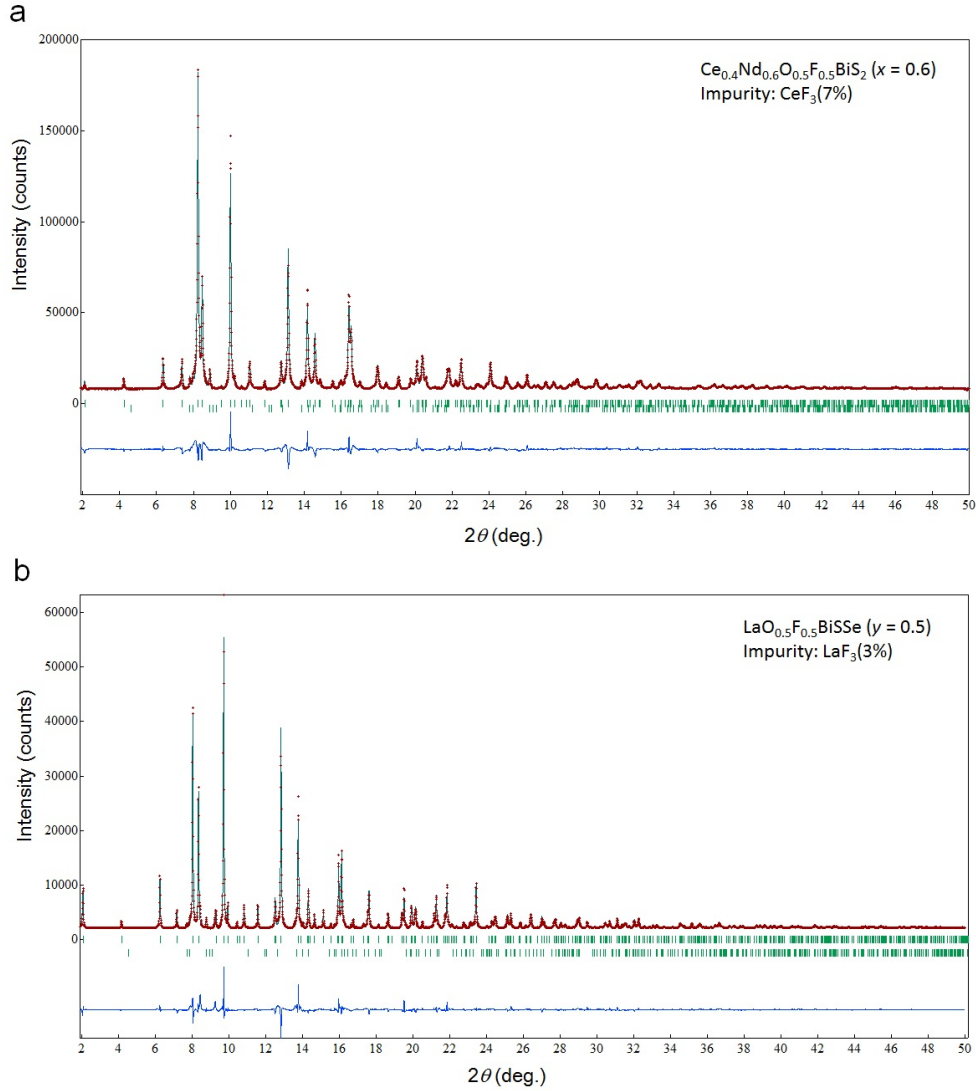


Fig. S1. Typical XRD patterns for $\text{Ce}_{1-x}\text{Nd}_x\text{O}_{0.5}\text{F}_{0.5}\text{BiS}_2$ and $\text{LaO}_{0.5}\text{F}_{0.5}\text{Bi}(\text{S}_{1-y}\text{Se}_y)_2$.

a. XRD patterns for $\text{Ce}_{0.4}\text{Nd}_{0.6}\text{O}_{0.5}\text{F}_{0.5}\text{BiS}_2$ ($x = 0.6$). The Rietveld refinement was performed including a CeF_3 impurity phase (7 %). The upper and lower bars indicate calculated peak positions for $\text{Ce}_{0.4}\text{Nd}_{0.6}\text{O}_{0.5}\text{F}_{0.5}\text{BiS}_2$ and CeF_3 , respectively. The reliable factor R_{wp} was 4.9%.

b. XRD patterns for $\text{LaO}_{0.5}\text{F}_{0.5}\text{BiSSe}$ ($y = 0.5$). The Rietveld refinement was performed including a LaF_3 impurity phase (3 %). The upper and lower bars indicate calculated peak positions for $\text{LaO}_{0.5}\text{F}_{0.5}\text{BiSSe}$ and LaF_3 , respectively. The reliable factor R_{wp} was 5.1%.

Table S1. Obtained crystal structure parameters.

Lattice constants a and c , z coordinate, occupancy of Se at Ch1 site ($g(\text{Se1})$), and reliable factor of Rietveld refinement (R_{wp}) for $\text{Ce}_{1-x}\text{Nd}_x\text{O}_{0.5}\text{F}_{0.5}\text{BiS}_2$, $\text{LaO}_{0.5}\text{F}_{0.5}\text{Bi}(\text{S}_{1-y}\text{Se}_y)_2$, $\text{Nd}_{0.8}\text{Sm}_{0.2}\text{O}_{0.5}\text{F}_{0.5}\text{BiS}_2$, and $\text{Nd}_{0.6}\text{Sm}_{0.4}\text{O}_{0.5}\text{F}_{0.5}\text{BiS}_2$ are listed. Atomic coordinate for the $\text{REO}_{0.5}\text{F}_{0.5}\text{BiS}_2$ series are RE(0, 0.5, z), Bi(0, 0.5, z), Ch1(0, 0.5, z), Ch2(0, 0.5, z), and O/F(0, 0, 0).

Composition	a (Å)	c (Å)	$z(\text{RE})$	$z(\text{Bi})$	$z(\text{Ch1})$	$z(\text{Ch2})$	$g(\text{Se1})$ (%)	R_{wp} (%)	Impurities
$\text{CeO}_{0.5}\text{F}_{0.5}\text{BiS}_2$	4.04119(7)	13.4736(3)	0.0975(1)	0.6249(1)	0.3810(6)	0.8136(5)	-	5.8	CeF_3 (9%)
$\text{Ce}_{0.8}\text{Nd}_{0.2}\text{O}_{0.5}\text{F}_{0.5}\text{BiS}_2$	4.0330(1)	13.4522(6)	0.0976(2)	0.6255(2)	0.3810(8)	0.8160(8)	-	5.8	CeF_3 (9%)
$\text{Ce}_{0.6}\text{Nd}_{0.4}\text{O}_{0.5}\text{F}_{0.5}\text{BiS}_2$	4.02710(8)	13.4510(8)	0.0965(1)	0.6249(1)	0.3792(6)	0.8131(5)	-	4.9	CeF_3 (8%)
$\text{Ce}_{0.4}\text{Nd}_{0.6}\text{O}_{0.5}\text{F}_{0.5}\text{BiS}_2$	4.01501(9)	13.4023(4)	0.0977(1)	0.6246(1)	0.3789(6)	0.8135(6)	-	4.9	CeF_3 (7%)
$\text{Ce}_{0.2}\text{Nd}_{0.8}\text{O}_{0.5}\text{F}_{0.5}\text{BiS}_2$	4.00682(9)	13.3997(4)	0.0969(1)	0.6248(1)	0.3780(7)	0.8130(6)	-	5.9	CeF_3 (3%) + NdF_3 (2%)
$\text{NdO}_{0.5}\text{F}_{0.5}\text{BiS}_2$	4.0017(1)	13.4166(5)	0.0973(2)	0.6249(2)	0.3762(9)	0.8117(8)	-	7.4	Bi_2S_3 (2%) + NdF_3 (5%)
$\text{Nd}_{0.8}\text{Sm}_{0.2}\text{O}_{0.5}\text{F}_{0.5}\text{BiS}_2$	3.99205(9)	13.4152(4)	0.0956(1)	0.6246(1)	0.3763(8)	0.8084(6)	-	7.6	unknown
$\text{Nd}_{0.6}\text{Sm}_{0.4}\text{O}_{0.5}\text{F}_{0.5}\text{BiS}_2$	3.9880(2)	13.4407(6)	0.0963(2)	0.6253(2)	0.377(1)	0.8088(8)	-	9.2	unknown
$\text{LaO}_{0.5}\text{F}_{0.5}\text{BiS}_2$	4.07063(6)	13.4848(3)	0.0978(1)	0.6237(1)	0.3797(6)	0.8103(5)	0.0	5.8	Bi_2S_3 (1%) + LaF_3 (7%)
$\text{LaO}_{0.5}\text{F}_{0.5}\text{BiS}_{1.8}\text{Se}_{0.2}$	4.07966(3)	13.4914(2)	0.09756(9)	0.62469(7)	0.3779(4)	0.8124(4)	17.3(5)	5.4	LaF_3 (4%)
$\text{LaO}_{0.5}\text{F}_{0.5}\text{BiS}_{1.6}\text{Se}_{0.4}$	4.09211(8)	13.5096(3)	0.0971(2)	0.6260(2)	0.3786(5)	0.8159(7)	36.7(8)	5.6	LaF_3 (9%)
$\text{LaO}_{0.5}\text{F}_{0.5}\text{BiS}_{1.4}\text{Se}_{0.6}$	4.10821(4)	13.5433(2)	0.0964(1)	0.62673(9)	0.3779(3)	0.8146(4)	54.2(5)	5.4	LaF_3 (4%)
$\text{LaO}_{0.5}\text{F}_{0.5}\text{BiS}_{1.2}\text{Se}_{0.8}$	4.12832(4)	13.5848(2)	0.0959(1)	0.62769(8)	0.3780(2)	0.8165(4)	73.4(5)	5.5	LaF_3 (3%)
$\text{LaO}_{0.5}\text{F}_{0.5}\text{BiSSe}$	4.13593(5)	13.6098(2)	0.0953(1)	0.6284(1)	0.3790(2)	0.8163(4)	87.9(5)	5.1	LaF_3 (3%)
$\text{LaO}_{0.5}\text{F}_{0.5}\text{BiS}_{0.8}\text{Se}_{1.2}$	4.14138(7)	13.6656(3)	0.0944(1)	0.6271(1)	0.3801(3)	0.8160(4)	97.9(7)	6.0	unknown